Supporting Information for: "Solar cell efficiency enhancement via light trapping in printable resonant dielectric nanosphere arrays"

Jonathan Grandidier[*,1], Raymond A. Weitekamp[1,2], Michael G. Deceglie[1], Dennis M. Callahan[1], Corsin Battaglia[3], Colton R. Bukowsky[1], Christophe Ballif[3], Robert H. Grubbs[2], and Harry A. Atwater[1]

[1] Thomas J. Watson Laboratories of Applied Physics, California Institute of Technology, Pasadena, CA 91125, USA
[2] Arnold and Mabel Beckman Laboratories of Chemical Synthesis, Division of Chemistry and Chemical Engineering, California Institute of Technology, Pasadena, CA 91125, USA
[3] Ecole Polytechnique Fédérale de Lausanne (EPFL), Institute of Microengineering (IMT), Photovoltaics and Thin Film Electronics Laboratory, 2000 Neuchâtel, Switzerland

Received 5 October 2012, revised 24 October 2012, accepted 24 October 2012
Published online November 2012

Keywords resonant dielectric structures, solar cells, nanospheres, photovoltaics, photonic crystal, amorphous silicon

* Corresponding author: e-mail jgrandid@caltech.edu, Phone: +1 (626) 395-2193, Fax: +1 (626) 844-9320

1 Silica nanosphere functionalization

Silica spheres of 700 nm diameter were obtained from Polysciences Inc. as a 10% (by weight) suspension in water. This suspension was filtered on a fine filtration frit, rinsed with tetrahydrofuran and acetone. The powder of spheres was washed with 10 mL of 1:1 methanol/HCl, and rinsed again with acetone. The mostly dried powder was then heated in an oven for 5 minutes at 110 °C and dried under vacuum overnight. To 25 mL toluene in a 50 mL round-bottomed flask, 786 mg of dry silica spheres were suspended and stirred. To this suspension was added 1 mL 3-aminopropyl(diethoxy)methyl silane. The suspension was stirred 72 hours, filtered on a fine frit, rinsed with toluene and dried in vacuo to yield 756 mg dry, amine-functionalized silica spheres.

2 Langmuir-Blodgett deposition

A ~1% (by weight) suspension for Langmuir-Blodgett deposition was prepared by suspending 235 mg of functionalized silica spheres in a solution of 4 mL ethanol and 17 mL methylene chloride. We first perform an isotherm measurement where we record the surface pressure of the water as a function of the surface area, which is reduced using the compression barriers of the LB trough. When the area of the trough is large, the surface pressure of the water is around 4 mN/m. The spheres are freely spread on the surface of the water. This is the so-called "gaseous" state. While the LB trough's barriers compress the spheres and reduce the area where the spheres stand on, the surface pressure slowly increases until 5 mN/m. The slope abruptly increases until 10 mN/m. This is the "liquid" state corresponding to a dense and condensed monolayer of hexagonally close packed spheres at the surface of the water. Upon further compression, the slope of the curve decreases and the monolayer collapses into multilayer structures. For our purpose, the optimal point is at the middle of the "liquid" condensed state where the spheres are well close packed and still form a monolayer. This point is reached when the surface pressure is around 7.5 mN/m. In a second step, knowing the optimal surface pressure for the deposition, we perform a dipping experiment. While the spheres are on the surface of the water in the "gaseous" state, we immerse the substrate into the LB trough. We then close the LB's barriers until the surface pressure reaches 7.5 mN/m. From that point, we slowly pull up the substrate at a rate of 1 mm/min while simultaneously keeping the surface pressure constant with a computer controlled feedback system between the electrobalance measuring of the surface pressure and the barrier moving mechanism. Consequently, the floating hexagonally close packed monolayer is adsorbed on the ITO surface. When the structure is totally removed from the water, the part that was initially immersed in the water is coated by a large area of nanoscale dielectric nanospheres on its entire surface.

3 Transfer printing preparation

Poly(vinyl alcohol) (avg. MW = 10,000 g/mol, 88% hydrolyzed, Sigma Aldrich) was spin cast from an aqueous solution containing 1 wt % PVA and 5 wt % gluteraldehyde onto the top glass surface of the cells with a thickness of 15-20

nm, as measured by ellipsometry. Poly(dimethylsiloxane) stamps were prepared from Sylgard 184 (1:10 curing agent : elastomer base, Dow Corning), poured into petri dishes to a thickness of ~5 mm and baked for 85 minutes at 80 °C. A 2D colloidal crystal of 700 nm diameter, aminated silica spheres was deposited on a glass slide, as described above. Spheres were transferred to the PDMS by firmly pressing the stamp into the colloidal array and carefully peeling it away. The stamp, now "inked" with spheres, was pressed against the PVA-coated surface by hand. The cells were placed in a large glass jar, which was purged with argon, covered with a large crystallization dish, and baked for 2 hours at 100 °C. The atmosphere was again purged with argon after the first hour. The jar containing the cells was removed and allowed to cool to room temperature. The PDMS stamps were carefully peeled away to render high fidelity colloidal crystals adhered to the PVA-coated glass surface, with good transfer yield.

4 Effective index model

We plot in Fig. S1 the simulation of EQE for the flat solar cell represented in Fig. 1 with a layer of 1.28 effective index corresponding to the equivalent occupied volume of the spheres and of the same thickness as the diameter of the spheres. Enhancement occurs in the blue part of the spectrum due to ARC effect. In the red part to the spectrum, EQE is equivalent to the solar cell without the additional layer. This confirms that the enhancement in the red part of the spectrum is due to resonant modes of the dielectric spheres as described in Fig. 3.

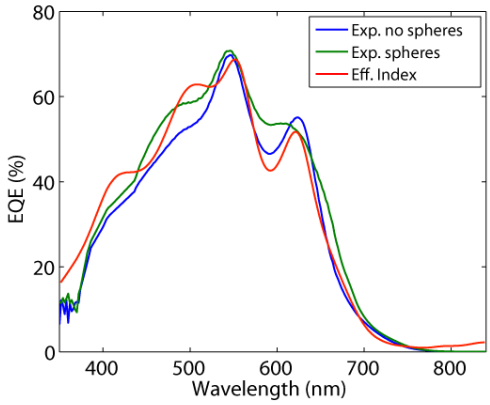

Figure S1 Effective index corresponding to the index of the spheres accounting for air and comparison with the measured data with and without the spheres.

5 Optical measurement on bare crystalline silicon

We also considered optically thick bare crystalline silicon (c-Si) with spheres on top (Fig. S2). This simple structure can be easily understood since distinct features due to resonant dielectric structures can be observed. We accounted for the size distribution of the spheres as described in the manuscript.

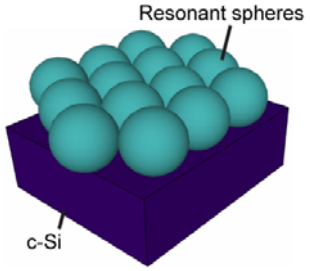

Figure S2 Schematic of the sphere array PV structure.

Optical characterization is used to measure the influence of the dielectric sphere monolayer array on the absorption in the photovoltaic structure. We performed reflection measurements as a function of wavelength and incidence angle using a motorized integrating sphere apparatus. A supercontinuum laser (Fianium) was coupled to a monochromator to provide a collimated illumination beam for a wavelength range between λ=400 nm and λ=1000 nm. The transmitted light through the c-Si layer can be neglected within that range, due to its thickness. As a reference, a reflection measurement at normal incidence was compared with a FDTD simulation of a bare semi-infinite c-Si layer [1]. From the reflection, we calculated the absorption (A = 1 - R). This is a valid approximation on an integrating sphere, which effectively captures all angles of

reflected light. We then measured the reflectance spectrum of the wafer with a sphere array on top, and simulated 21 FDTD cases for sphere diameters between 615 nm and 715 nm. Each simulation assumes an infinite array of spheres with periodic boundary conditions. In order to account for the experimentally measured distribution of the sphere size, we weighted the set of simulations by the Gaussian distribution. This weighted average fits the measured absorption well, and its median diameter of 665 nm. The resonant features of the experimental spectrum and the weighted average spectrum are very well matched (Fig. S3b). We attribute the difference in the measured intensity to the fact that in the experiment, sizes of spheres are randomly distributed on a single sample whereas we combined a weighted set of simulations, each of a single sphere size.

In order to analyze each of the features in the measured reflection curve, we also plot the result of the simulation of the median diameter of 665 nm in Fig. S3b. Its resonant response is similar to that of the simulated average and measured curves. Three sharp and distinct peaks are observed and labeled c, d, and e. For each of these peaks, we plot the electric field intensity for a cross section at the middle of a sphere in the same plane as the polarization of the normal incident plane wave. We verified experimentally and theoretically [2] that the absorbed power is independent of the polarization at normal incidence. The features in the absorption spectra are clearly associated with the excitation of resonant modes of the nanospheres [3]. Directly under the modal profile of the spherical cross section, we plot the electric field intensity in the first 300 nm of c-Si both with and without the nanosphere array, at the corresponding wavelengths. It is clearly seen that the electric field intensity is greater in the c-Si layer with the resonant dielectric structures on top. This result demonstrates that the excitation of resonant modes within a dielectric structure can have a significant impact on the absorption enhancement of a photovoltaic structure. In our measurement, the total relative absorption enhancement measured is about 9%.

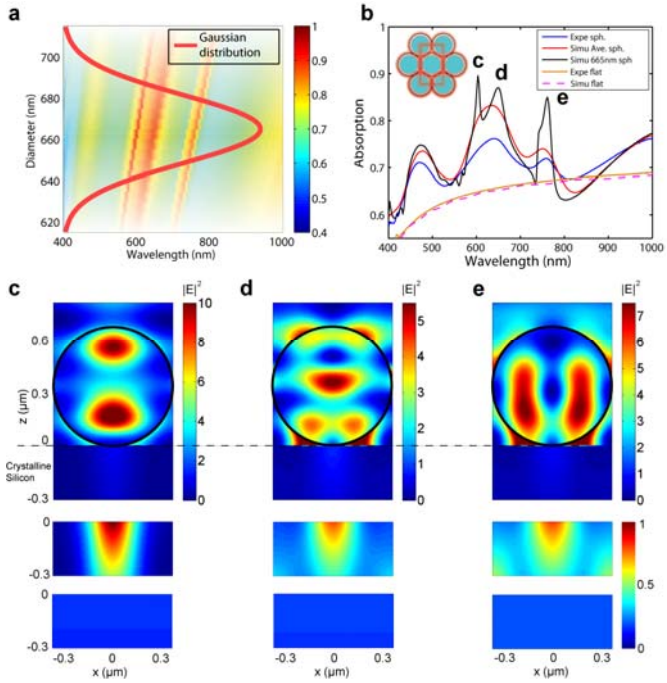

Figure S3 (a) Map of the absorption as a function of the wavelength for the different sphere diameters across the measured size distribution. The Gaussian distribution of sphere diameters, used to weight each individual simulations, is plotted on top, with arbitrary amplitude. (b) Simulated and measured absorption for the photovoltaic structure with dielectric spheres on top of it. (c,d,e) For each labeled peak on b: electric field intensity for a cross section at the middle of a sphere. Below on a different color scale is the electric field intensity for a cross section within the first 300 nm of absorbing layer and below that, the equivalent case without spheres.

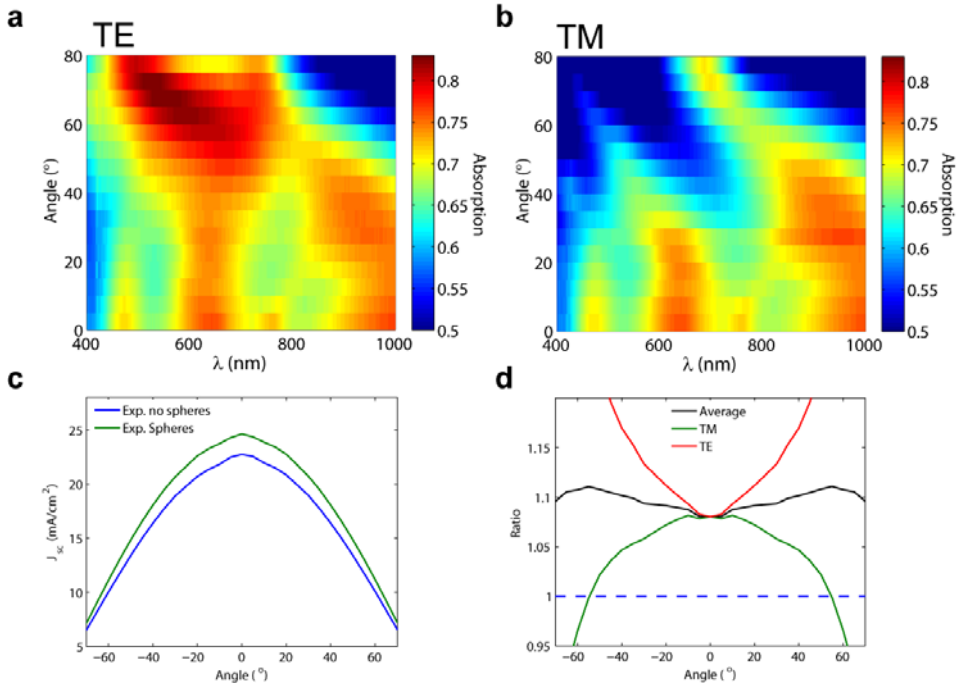

Figure S4 Angle resolved measurement of the absorption for a (a) transverse electric and (b) transverse magnetic polarization. (c) Jsc generated by the active material for the case with and without spheres. TE and TM polarization were averaged to account for the isotropic radiation of the sun. The solar irradiance that was used to weight the measured absorption [4]. (d) Relative absorption enhancement over the bare structure as a function of the incident angle.

We then measured the angle dependence of the absorbed light in both transverse electric (TE) and transverse magnetic (TM) polarizations (Fig. S4a and b). The observed absorption bands account for the variation of the resonant dielectric structure as a function of the angle of incidence. In order to evaluate the performance of the considered photovoltaic structure, we interpolated angle-resolved data [4] of the incident solar energy on a sunny day to match resolution of our absorption measurements represented in Fig. S4a and b. The TE and TM measurements are averaged and weighted by the interpolated data of the sun's energy. We then calculated the relative absorption enhancement due to the colloidal crystal (Fig. S4d). The enhancement is relatively constant with an average of almost 10%. Interestingly, the strongest enhancement of 11.21% is measured for an angle of 55°. The angle-independent enhancement is a promising result; it demonstrates that these resonant dielectric structures can couple direct and indirect sunlight throughout the day.

6 Graded-index model: transfer matrix simulations

To support our proposed light-trapping mechanism via PC modes, we performed 1D transfer matrix simulations [5] to account for the graded index effects of the colloidal geometry. Because these 1D simulations cannot account for 3D modes, it provides a useful complement to our 3D FDTD simulations. For the transfer matrix simulations, the spheres were divided into 100 layers, each with an effective index corresponding to the volume fraction of glass in air. Two simulations (Fig. S5) demonstrate the calculated effects of these dielectric structures in the near- and far-field cases.

Figure S5a shows the simulated absorption of an array of silica spheres on a c-Si wafer (Fig. S2) using each method, both averaged over 21 simulations as previously described, and for the mean sphere diameter. While the averaged simulations qualitatively share features, the absorption peak near 750 nm cannot be accounted for using the transfer matrix method. This peak corresponds to the strongest PC mode resonance, which has been aligned with the amorphous silicon absorption profile by design. This provides further evidence that the observed absorption enhancement is due to the proposed PC mode coupling, and not simply a graded index effect due to the sphere geometry. The FDTD simulations were supported by experiment (see the previous section).

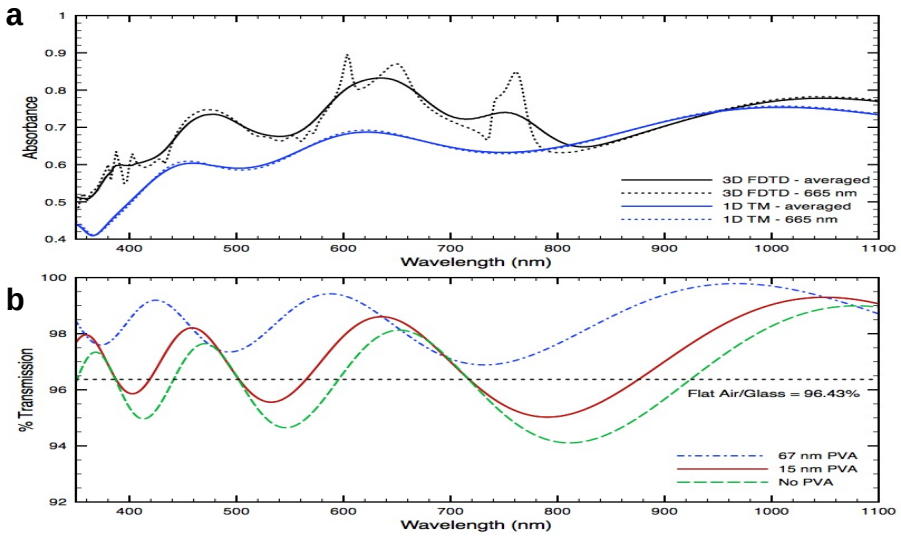

Figure S5 (a) 3D FDTD simulations are compared to 1D transfer matrix simulations for a graded index array approximating a silica sphere with 665 nm diameter. The main resonance is not observed in the transfer matrix simulations, as expected. (b) A graded index array approximating a 700 nm diameter sphere is simulated, with various thicknesses of PVA surrounding the base of the sphere.

To simulate the graded-index effect of the spheres for the ZnO/a-Si:H/ ZnO cell structure, where the spheres are separated from the active layer by 0.5 mm of SiO_2, we simulated the modified transmission of light at the air/glass interface. The simulations reveal that the graded index profile of the silica sphere and PVA surrounding the base provide an antireflective coating for the air/glass interface. The PVA has an index very close to that of glass, and was taken as equal to glass (n = 1.466) for these simulations. The thickness of the PVA layer was nominally ~15 nm before the spheres were transfer printed onto the surface. Because the PVA is simultaneously being heated above its glass transition temperature and cross-linked with gluteraldehyde, the thickness of the PVA after the spheres are embedded is difficult to determine. If the density of the PVA remains unchanged, and the sphere is fully embedded in the layer, the corresponding height of the PVA layer would be 67 nm due to the excluded volume of the sphere. Thus, we take 15 and 67 nm as the upper and lower bounds for PVA thickness. We can see in the figure that transmission into the glass is improved at the wavelengths where we experimentally observed improvement in the EQE (Fig. 4c), between ~400-500 nm and ~600-700nm.

7 Angle measurements on a flat solar cell

We show in Fig. S6 the experimental measurements of the EQE. We also plot the simulated EQE using RCWA angle dependent characterization. For the simulations, we considered for both TE and TM polarizations, and k_x and k_y directions. These measurements and simulations were used as an input for Fig. 4a and b of the main manuscript.

EXPERIMENT

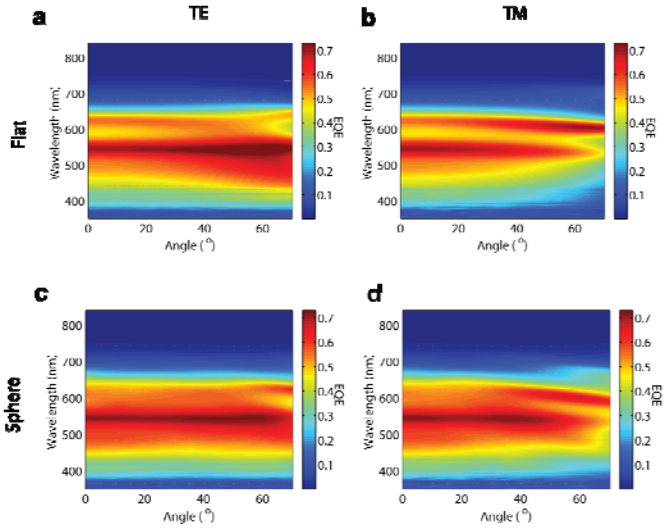

SIMULATION

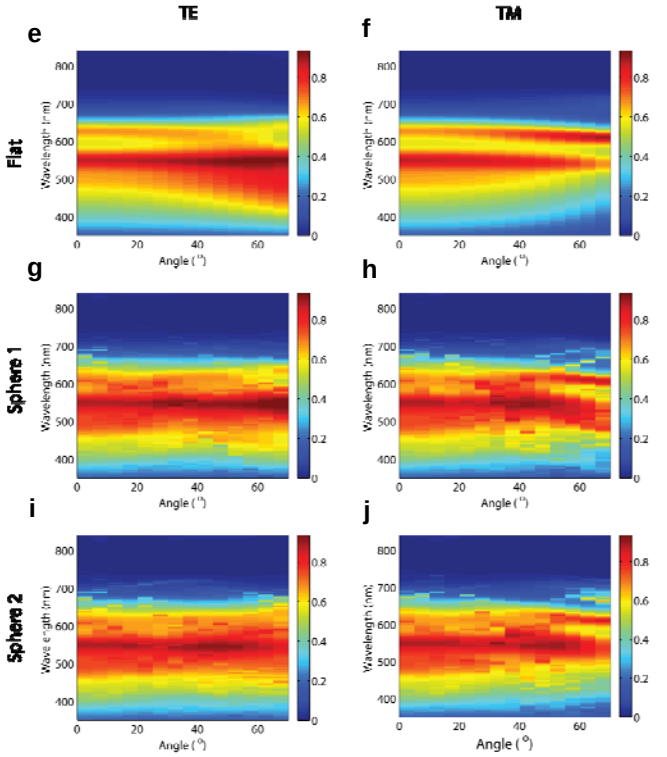

Figure S6 Angle resolved measurement of the EQE for a (a) transverse electric and (b) transverse magnetic polarization for a flat solar cell and for a solar cell with spheres on top (c,d). Angle resolved simulation using RCWA of the EQE for a (e) transverse electric and (f) transverse magnetic polarization for a flat solar cell and for a solar cell with spheres on top considering k_x (g,h) and k_y (i,j) directions.

8 Optical parameters

As an input for the 3D FDTD and RCWA simulations, optical constants of all materials were measured by spectroscopic ellipsometry, except aluminum, for which they were taken from Palik [1]. The method employed here for calculating EQE from optical simulations assumes each absorbed photon creates a mobile electron hole pair, which is subsequently collected with unity efficiency. Since these assumptions may not hold for an experimental a-Si:H device, a wavelength independent collection efficiency of 0.8 was assumed to fit the experimental data (Fig. 2a and 3b). The thicknesses were adjusted slightly for each layer to reproduce the EQE of the flat cell without spheres.

9 Electrical measurement

A supercontinuum laser (Fianium) was coupled to a monochromator to provide collimated illumination between 350 and 840 nm. A beam splitter was employed to direct part of the beam to a reference photodiode, to account for real-time fluctuations in source intensity. To calibrate the ratio of light incident on the reference diode and sample, we also performed the EQE measurement with a NIST traceable calibrated photodiode with known EQE in the sample position. The laser beam width was about 1 mm, which is smaller than the area of the solar cells and the calibrated diode, enabling area-independent measurements. Moreover, on the length scale of nanospheres, the laser beam approximates a plane wave.

10 Electrical parameters

The electrical parameters for the device physics simulation (Fig. 2b) were taken from Schropp and Zeman [6], with the exceptions that all the a-Si:H layers have an assumed bandgap of 1.78 eV, electron affinity of 4 eV, a relative permittivity of 11.9, and the peak dangling bond concentration in the intrinsic region was set to 5×10^{17} cm^{-3}. In addition, we added a distributed series resistance of 15 Ω cm^2 to reproduce the slope of the current-voltage curve near open circuit. We also found it necessary to scale down the generation rate calculated by FDTD by a multiplicative factor of 0.9 to match the experimental IV curve, this increase from the factor of 0.8 used in the analysis of the optical simulations is justified by noting that the device physics simulation accounts for imperfect carrier collection.

References

[1] E. D. Palik and G. Ghosh, Handbook of Optical Constants of Solids (Academic Press, 1998).
[2] J. Grandidier, M. G. Deceglie, D. M. Callahan, and H. A. Atwater, J. Photon. Energy **2**, 024502 (2012).
[3] J. Grandidier, D. M. Callahan, J. N. Munday, and H. A. Atwater, Adv. Mater. **23**, 1272-1276 (2011).
[4] B. Marion, B. Kroposki, K. Emery, J. del Cueto, D. Myers, and C. Osterwald, Validation of a photovoltaic module energy ratings procedure at NREL, Technical report NREL/TP-520-26909 (1999).
[5] S. J. Orfanidis, Electromagnetic Waves and Antennas http://www.ece.rutgers.edu/~orfanidi/ewa/, May 2012.
[6] R. E. I. Schropp and M. Zeman, Amorphous and Microcrystalline Silicon Solar Cells: Modeling, Materials, and Device Technology: (Kluwer Academic, Norwell MA, 1998).